Journal of Power Sources 300 (2015) 112–122

Contents lists available at ScienceDirect

Journal of Power Sources

journal homepage: www.elsevier.com/locate/jpowsour

Modeling mechanical degradation in lithium ion batteries during cycling: Solid electrolyte interphase fracture

Izaro Laresgoiti [a, b, *], Stefan Käbitz [a, b], Madeleine Ecker [a, b], Dirk Uwe Sauer [a, b, c]

[a] Chair for Electrochemical Energy Conversion and Storage Systems, Institute for Power Electronics and Electrical Drives (ISEA), RWTH Aachen University, Jaegerstrasse 17-19, 52066 Aachen, Germany
[b] Juelich Aachen Research Alliance, JARA-Energy, Germany
[c] Institute for Power Generation and Storage Systems (PGS) @ E.ON ERC, RWTH Aachen University, Germany

HIGHLIGHTS

- A degradation model based on the fracture and reparation of the SEI is presented.
- Active material and SEI fracture are treated as different aging mechanisms.
- The model is validated against cycle life tests from commercial 18650 cells.
- The model reproduces the influence of the DOD and SOC_{mean} on the capacity fade.

ARTICLE INFO

Article history:
Received 25 June 2015
Received in revised form
25 August 2015
Accepted 8 September 2015
Available online 25 September 2015

Keywords:
Lithium ion
Mechanical degradation
Diffusion induced stress
Solid electrolyte interphase
Cycle aging
Lifetime estimation

ABSTRACT

During cycling, mechanical stresses can occur in the composite electrode, inside the active material, but also in the solid electrolyte interphase layer. A mechanical model is proposed based on a system made of a spherical graphite particle surrounded by the solid electrolyte interphase layer. During lithium intercalation or de-intercalation, stresses in the graphite are produced, governed by the diffusion induced stress phenomena and in the solid electrolyte interphase, driven by the graphite expansion. The stresses in both materials were simulated and a sensitivity analysis was performed to clarify the influence of principal parameters on both processes. Finally, assuming that the solid electrolyte interphase is the weakest material and therefore more prone to fracture than graphite, the experimental capacity fade during cycling was modeled based on its break and repair effect rather than on the fracture of the active material. The mechanical model of the solid electrolyte interphase was implemented in a single particle lithium ion battery model in order to reproduce capacity fade during battery lifetime. The model results were compared against cycle life aging experimental data, reproducing accurately the influence of the depth of discharge as well as the average state of charge on the capacity fade.

1. Introduction

The increase of research and development of new materials and manufacturing processes in Li-ion batteries, due to the rapid increase of the electric vehicle market, have improved significantly their performance in terms of energy and lifetime. Many works dealing with the aging of lithium ion batteries have been published constantly, nevertheless many questions are still open nowadays. When it comes to aging due to calendaric conditions, the scientific community has agreed that side reactions occurring between the electrolyte and the electrodes [1–3] are responsible for the degradation of the battery, which is accelerated at high temperature and high state of charges (SOC) [4].

However, addressing cycle aging is significantly more challenging since the side reactions interact with volume changes and temperature gradients in the cell. The interaction of such phenomena is not completely understood nowadays. In addition, the influence of stress factors such as C-rate, depth of discharge (DOD) and average state of charge (SOC_{mean}) is not fully determined.

It is generally accepted that the mechanical degradation is a key

* Corresponding author. Chair for Electrochemical Energy Conversion and Storage Systems, Institute for Power Electronics and Electrical Drives (ISEA), RWTH Aachen University, Jaegerstrasse 17-19, 52066 Aachen, Germany.
E-mail addresses: batteries@isea.rwth-aachen.de, ila@isea.rwth-aachen.de (I. Laresgoiti).

http://dx.doi.org/10.1016/j.jpowsour.2015.09.033
0378-7753/

factor to understand the cyclic aging of lithium ion batteries. To date, cycle aging has been addressed based on the Diffusion Induced Stress (DIS) principle. In 2006 Christensen [5,6] presented the DIS formalism as driving force for particle fracture in carbon and $LiMn_2O_4$ particles. He reported that the maximum stress increases with the C-rate and particle size. Later on, the same author [7] and Renganathan et al. [8], investigated stress generation in porous electrodes. Many of the published literature deal with the improvement of the accuracy of the stresses investigating the influence of the particle shape [9], phase changes [10] or variable Young modulus [11] on the observed stresses, among others.

But recently, several investigations [12,13] have been carried out where the capacity fade during cycling was reproduced using a phenomenological model based on the DIS phenomena and a fatigue approach. The model re-creates the fracture of the graphite particles and subsequent reduction of the electrolyte in the newly exposed surfaces neglecting the solid electrolyte interphase (SEI) fracture. However, a recently published paper [14] reveals that the fracture of the particles does not occur unless very severe conditions are applied, such as very low temperatures (down to −10 °C). Hence, the possibility that exclusively SEI fracture occurs must be investigated. The fracture of the SEI can lead to the reduction of the electrolyte (that penetrates through the cracks) regenerating the SEI and henceforth increasing its thickness. This approach seems to be reasonable since the SEI is a non-homogeneous porous material [15–17] easier to fracture than the graphite. The mechanical behavior of the SEI has not been studied numerically so far to the author's knowledge although the scientific community is aware of its importance in the cycle life stability. Purewal et al. [13] mentioned that the effect of the SEI was implicitly explored in their model resulting in a small alteration of the mechanical parameters of the graphite material. However, despite active material stress and SEI stress apparently being equivalent phenomena, their investigation must be carried out separately because they lead to very diverse effects.

This paper presents a novel approach to explain and model the capacity fade behavior during battery cycling and which is able to clarify the influence of the stress factors in the capacity fade (C-rate, DOD and SOC_{mean}). Based on the reasons given previously, in our approach the active material damage due to DIS (Fig. 1a)) is believed to have a minor effect on degradation of the cell, leaving the SEI damage (Fig. 1b)) as the main aging mechanism contributing to the capacity fade.

The presented model was validated with experimental data obtained from extensive accelerated aging tests performed on Li-ion Sanyo high energy 18650 cells of 2.05 Ah and presented in Ref. [4]. The model was able to reproduce the DOD influence and the SOC_{mean} influence on the capacity fade and thus presents an explanation for such behavior.

2. Experimental

In our previous work [4], a large collection of cycle aging data was presented for a graphite/NMC HE 18650 Sanyo cell. The cycle aging was thoroughly analyzed stressing the SOC_{mean} and DOD influence on the capacity fade. All the tests were carried out at 1 C symmetric charge discharge cycles and 35 °C (cell temperature). The cycling was always performed at constant current conditions and the DOD was defined by the Ah throughput in respect to the nominal capacity. On the one hand, the cycle depth influence on the capacity was studied performing cycle tests at 50% SOC_{mean}. On the other hand, the SOC_{mean} influence was investigated performing the cycle tests at 10% DOD and 20% DOD. The capacity of the cell was controlled performing standard charging (constant current followed by a constant voltage) followed by a 1 C discharge every 3 weeks. A summary of the investigated tests is shown in Table 1.

3. Modeling

3.1. Mechanical model: SEI and active material system

The SEI layer is a porous multicomponent material produced as the result of the irreversible decomposition of the electrolyte with carbon materials. Its exact composition is not completely elucidated. However, the non-homogeneous nature of the layer is accepted [18]. SEI is presented as a several Å to tens or hundreds of Å [15] thick layer surrounding the active material particle that is subjected to the volume change during the de-intercalation and intercalation of the lithium ions. Due to continuous expansion and compression of the material, the SEI layer could be damaged affecting the cycle life considerably.

A similar mathematical concept was presented by Hao et al. [19] where core–shell nanostructures stresses were investigated with the aim of enhancing the electronic conductivity of the electrode materials. Fig. 1c) shows the proposed model geometry composed of a spherical active material particle surrounded by the SEI shell.

When the dimension of the system under study goes below tens of nanometers, surface stresses and energies acquire a great importance on the mechanical properties of the materials. The influence of the surface stresses on the DIS has been mathematically investigated by Hao et al. [19] and by Cheng et al. [20]. Strictly speaking, for the micrometer size active material particle, this phenomena can be neglected but not for the nanometer size SEI layer. However, since the aim of our investigation is not the accurate calculation of the stresses, but their qualitative comparison at different working conditions of the battery, for simplicity, the surface effect has been neglected. Additionally, for mathematical simplicity a homogenous SEI layer was assumed.

The stress due to intercalation/de-intercalation of lithium ions in the active material is derived equivalently to the temperature induced stress and it is widely known as diffusion induced stress that is explained in Refs. [5–9], among others. The expression relating the strain and the stress for an elastic body and for the particular case of a spherical symmetry reads as follows:

$$\varepsilon_r = \frac{1}{E}[(1+\nu)\sigma_r - \nu\sigma_t] + \frac{c\Omega}{3} \tag{1}$$

$$\varepsilon_t = \frac{1}{E}[(1-\nu)\sigma_t - \nu\sigma_r] + \frac{c\Omega}{3} \tag{2}$$

where ε_r and ε_t are the radial and tangential strain respectively, σ_r and σ_t the radial and tangential stresses, E the Young modulus, ν the Poisson's ratio, c the concentration inside the active material particle and Ω the partial molar volume of the solute in the solid material (which describes the volume of a mol of lithium when it intercalates into the graphite).

It is assumed that the material is isotropic and any variation in the elastic properties with Li concentration has been neglected. Additionally, no external forces acting on the surface of the particle is assumed, resulting on the following equilibrium equation for the stress tensor:

$$\frac{d\sigma_r}{dr} + \frac{2(\sigma_r - \sigma_t)}{r} = 0 \tag{3}$$

The strain tensor is related to the displacement tensor u by the following expressions:

$$\varepsilon_r = \frac{du}{dr},\ \varepsilon_t = \frac{u}{r} \tag{4}$$

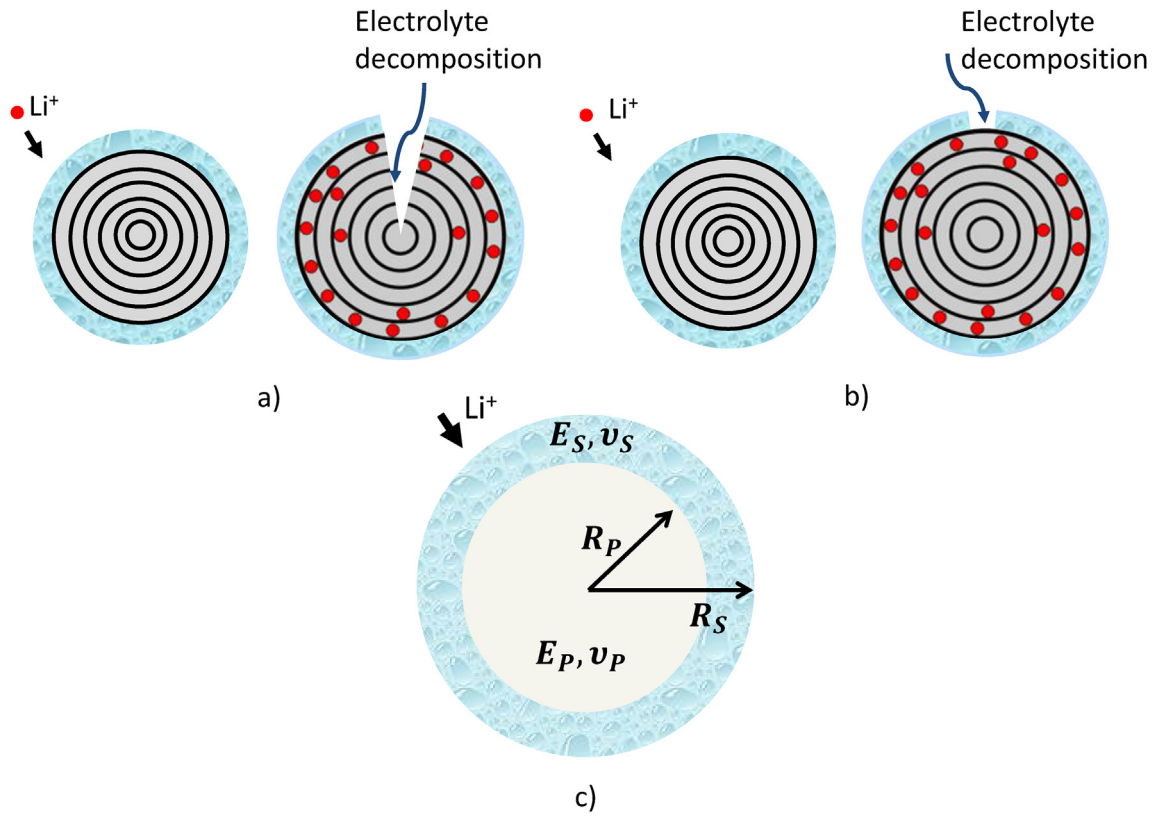

Fig. 1. a) Particle fracture due to DIS phenomenon, b) SEI fracture, c) Active material and SEI layer system with the main parameters used in the model.

Substituting the strain-displacement relations Eq. (4) into the Eqs. (1) and (2) and finally replacing σ_r and σ_t in Eq. (3), results in the following 2nd order displacement differential equation:

$$\frac{d^2u}{dr^2}+\frac{2}{r}\left(\frac{du}{dr}\right)-2\frac{u}{r^2}=\frac{1+\nu}{1-\nu}\frac{\Omega}{3}\frac{dc}{dr} \tag{5}$$

where the concentration c in the particle varies with the particle radius.

The analytical solutions for the presented differential equation in the two domains are:

$$u_P(r)=\frac{(1+\nu_P)}{(1-\nu_P)}\frac{\Omega_P}{3}\frac{1}{r^2}\int_0^r c_P\, r^2 dr + a_P\, r + \frac{b_P}{r^2} \tag{6}$$

Table 1
Test matrix with the testing conditions.

T (°C)	35				
C-Rate	1				
ΔDOD (%)	100	50	20	10	5
SOC-Range (%)	0–100	25–75	80–100 65–85 40–60 15–35 0–20	90–100 85–95 70–80 45–55 20–30 5–15	47.5–52.5

$$u_S(r)=\frac{(1+\nu_S)}{(1-\nu_S)}\frac{\Omega_S}{3}\frac{1}{r^2}\int_0^r c_S\, r^2 dr + a_S\, r + \frac{b_S}{r^2} \tag{7}$$

where sub index P refers to the variables in the active material and S to the variables in the SEI layer. Additionally, a_P, b_P, a_S and b_S are constant of integration to be defined by the boundary conditions.

By substituting the Eq. (4) into (1) and (2) the stress can be expressed in terms of the displacement as follows:

$$\sigma_r=\frac{E}{(1+\upsilon)(1-2\upsilon)}\left[(1-\nu)\frac{du}{dr}+\frac{2\nu u}{r}-(1+\nu)\frac{c\Omega}{3}\right] \tag{8}$$

$$\sigma_t=\frac{E}{(1+\upsilon)(1-2\upsilon)}\left[\nu\frac{du}{dr}+\frac{u}{r}-(1+\nu)\frac{c\Omega}{3}\right] \tag{9}$$

Finally, the displacement Eqs. (6) and (7) are integrated into Eqs. (8) and (9) and the following equations for the radial (presented with r sub index) and tangential stress (presented with t sub index) are obtained in the active material:

$$\sigma_{rP}(r)=-\frac{2\Omega_P E_P}{3(1-\nu_P)}\frac{1}{r^3}\int_0^r c_P\, r^2 dr+\frac{E_P}{(1-2\nu_P)}a_P-\frac{2}{r^3}\frac{E_P}{(1+\nu_P)}b_P \tag{10}$$

$$\sigma_{tP}(r) = \frac{\Omega_P E_P}{3(1-\nu_P)}\frac{1}{r^3}\int_0^r c_P\, r^2 dr + \frac{E_P}{1-2\nu_P}a_P + \frac{1}{r^3}\frac{E_P}{1+\nu_P}b_P - \frac{\Omega_P\, E_P c_P}{3(1-\nu_P)} \tag{11}$$

Considering that there is no expansion ($\Omega_S = 0$) of the SEI itself due to particle charge and discharge, the equations for the stresses in the SEI (σ_{rS} and σ_{tS}) are considerably simplified:

$$\sigma_{rS}(r) = \frac{E_S}{1-2\nu_S}a_S - \frac{2}{r^3}\frac{E_S}{1+\nu_S}b_S \tag{12}$$

$$\sigma_{tS}(r) = \frac{E_S}{1-2\nu_S}a_S + \frac{1}{r^3}\frac{E_S}{1+\nu_S}b_S \tag{13}$$

4 Integration constant a_P, b_P, a_S and b_S must be determined applying the following boundary conditions:

- The displacement in the center of the particle is zero:

$$u_P(r=0) = 0 \tag{14}$$

- Because of the mechanical equilibrium, the radial stress on the surface of the particle must be zero:

$$\sigma_{rS}(r = R_S) = 0 \tag{15}$$

- Both materials are assumed to be perfectly bonded (i.e. the displacement must be continuous across the boundary)

$$u_P(r = R_P) = u_S(r = R_P) \tag{16}$$

- The radial stress must be continuous through the boundary:

$$\sigma_{rP}(r = R_P) = \sigma_{rS}(r = R_P) \tag{17}$$

The final equations together with the boundary conditions bring us to the following system of linear equations:

$$a_P - a_S - \frac{b_S}{R_P^3} = -\frac{(1+\nu_P)}{(1-\nu_P)}\frac{\Omega_P}{3}\frac{1}{R_P^3}\int_0^{R_P} c_P\, r^2\, dr \tag{18}$$

$$\frac{a_S}{1-2\nu_S} - \frac{2}{R_S^3}\frac{b_S}{(1+\nu_S)} = 0 \tag{19}$$

$$-\frac{E_P a_P}{1-2\nu_P} + \frac{E_S a_S}{1-2\nu_S} - \frac{2}{R_P^3}\frac{E_S b_S}{(1+\nu_S)} = -\frac{2\Omega_P E_P}{3(1-\nu_P)}\frac{1}{R_P^3}\int_0^{R_P} c_P\, r^2\, dr \tag{20}$$

In case of a Ω_P which varies with the lithium concentration, it must be introduced in the integral:

$$\Omega_P \int_0^{R_P} c_P\, r^2\, dr = \int_0^{R_P} r^2\, dr \int_0^{c_P} \Omega_P\,(c_p)\, dc_P \tag{21}$$

Eqs. (18–20) comprise a system of linear equations from which a_P, a_S and b_S can be computed. Substituting the integration constants in the Eqs. (10–13) the stresses in the active material and the SEI can be obtained respectively.

3.2. Fatigue approach

During normal working conditions, and for electrodes made of common intercalation materials, where the volume increase during intercalation is always smaller than 10%, the stresses in some cases do not reach the yield strength of the material [5,13]. However, during operation of the battery the material is subjected to cyclic loading. Due to this repetitive loading microscopic structural damage can accumulate leading to the fracture of the particles even if the loads are considerably lower than the yield strength of the material.

The probabilistic S–N curve (Wöhler curve) [21] can be very useful to predict the material fracture under cyclic loading, where the effect of the microscopic damage of the material is implicitly included. These curves are based on statistical data obtained experimentally and they relate the number of life cycles that a material can withstand to the amplitude of the cyclic stress. The amplitude of the cyclic stress is calculated using the following equation:

$$\sigma_{ampl} = \frac{\sigma_{Max} - \sigma_{Min}}{2} \tag{22}$$

where σ_{Max} and σ_{Min} are the maximum and minimum stress values of the cyclic signal respectively.

In a bi-logarithmic graph, the Wöhler curve can be approximated by a straight line [21], which represents that with lower stress amplitudes the material is able to withstad more cycles:

$$log\sigma_{ampl} = log\sigma_{Yield} - m log N \tag{23}$$

Thus the "Basquin" power law can be used to calculate the maximum number of cycles to failure (N_{Max}) [21]:

$$N_{Max} = \left(\frac{\sigma_{Yield}}{\sigma_{ampl}}\right)^{\frac{1}{m}} \tag{24}$$

where σ_{Yield} is the stress at static failure (or maximum yield strength) and m the slope of the σ_{ampl} vs. N curve in the bi-logarithmic diagram, both being material specific parameters.

Thus, for a given stress amplitude, Eqs. (22) and (24) provide a way to calculate the maximum number cycles to failure.

Unfortunately, the S–N curves are only available for the best known structural materials such as aluminium, steel, etc. For the materials used in batteries, such as graphite or the SEI, some guess work is needed. For instance, the slope in the S–N curve has to be guessed. Despite this uncertainty in the fatigue parameters, it is worth to apply the formalism even without knowing the precise parameters for the curve because it allows us to analyze the impact of different operating strategies and electrode designs on the aging of cells. Without a parameterised curve we can not predict exact lifetimes in terms of number of cycles. This would require anyhow detailed models of all aging processes, but we can predict how different designs and operating conditions will alter the expected lifetime.

For materials subjected to complex loading (different cyclic stresses), Palmgren Miner [22] proposed the following linear equation relating the cumulative damage D to the loads and number of cycles applied, which is valid if single stress events are independent from each other:

$$D = \sum_{i=1}^{k} \frac{n_i\left(\sigma_{ampl\ i}\right)}{N_{Max\ i}} \tag{25}$$

where $n_i(\sigma_{ampl\ i})$ is the number of applied cycles subjected to $\sigma_{ampl\ i}$ stress and $N_{Max\ i}$ is the number of cycles to failure at $\sigma_{ampl\ i}$, calculated from the Eq. (24). Thus, each of the added $n_i(\sigma_{ampl\ i})/N_{Max\ i}$ fractions gives a contribution to the total degradation. Similar to other cumulative damage forms, when the sum reaches one the fracture of the material is assumed. Miner's rule enables us to calculate the contribution of each cycle to the degradation of the electrode.

Substituting N_{Max} from Eq. (24) in Eq. (25) the following expression can be obtained:

$$D = \sum_{i=1}^{k} \left(\frac{\sigma_{ampl\ i}}{\sigma_{Yield}}\right)^{\frac{1}{m}} n_i\left(\sigma_{ampl\ i}\right) \tag{26}$$

Accelerated aging tests are performed under uniform stress conditions, where $\sigma_{ampl\ i}$ remains constant during the cycle test. This fact permits the removal of the $n_i(\sigma_{ampl\ i})$ in the Eq. (26) leading to the following simplified expression:

$$\frac{D}{Cycle} = \left(\frac{\sigma_{ampl}}{\sigma_{Yield}}\right)^{\frac{1}{m}} \tag{27}$$

Thus, generally, the degradation per cycle is an expression dependent on the Yield strength of the material, the amplitude of the stress that the material is subjected to and m, fatigue strength exponent which describes the influence of the stress amplitude on material fracture.

Since the resistance increase presented in the experimental data [4] is small and the battery is built for high energy applications, its lifetime is limited due to capacity loss rather than resistance increase. Thus, damage D in this particular case of cyclic aging is assumed to be analogous to the capacity loss (Cap^T_{loss} (%)).

$$\frac{D}{Cycle} = \left(\frac{\sigma_{ampl}}{\sigma_{Yield}}\right)^{\frac{1}{m}} \propto \frac{Cap^T_{loss}(\%)}{Cycle} \tag{28}$$

The total capacity loss can be expressed as the sum of the capacity loss occurring due to the calendaric aging and the capacity loss due to cyclic aging [23]:

$$\frac{Cap^T_{loss}\ (\%)}{Cycle} = \frac{Cap^{CAL}_{loss}(\%)}{Cycle\ (h)} + \frac{Cap^{CYC}_{loss}(\%)}{Cycle} \tag{29}$$

In the particular case of Sanyo HE cell, at 35 °C, calendaric aging contribution to the total degradation during cyclic aging can be neglected [23]. Therefore, the total capacity loss can be approximated as:

$$\frac{Cap^T_{loss}\ (\%)}{Cycle} \approx \frac{Cap^{CYC}_{loss}(\%)}{Cycle} \tag{30}$$

From Eq. (28), it can be derived that the capacity loss during cycling is proportional to the stress amplitude to which the material is subjected to:

$$\frac{Cap^T_{loss}\ (\%)}{Cycle} \approx \frac{Cap^{CYC}_{loss}(\%)}{Cycle} = A_1 \left(\frac{\sigma_{ampl}}{\sigma_{Yield}}\right)^{\frac{1}{m}} \tag{31}$$

where A_1 is a factor that quantifies the capacity loss (in percentage) in case that SEI fracture and reparation occurs in every cycle. Under this assumption, when the stress amplitude approaches zero, the cycling capacity loss approaches zero and thus the calendaric contribution cannot be neglected anymore.

3.3. Integration to the Li-ion model and parameterization

The presented mechanical model has been integrated in a single particle Li-ion model [24,25]. Each electrode is characterized by a single particle, neglecting the concentration gradients in the electrolyte as well as the potential gradients in the solid phase. The adopted approach has been considered, since the goal of the investigation focuses on the mechanical behavior of the electrodes under certain stress factor (i.e. DOD and SOC_{mean}) rather than a detailed spatially resolved stress prediction.

To model the behavior of the electrodes correctly it is necessary to know the balancing of the cell. Actually, the cell balancing refers to the ratio between anode capacity and the cathode capacity in a full battery. A proper cell balancing is essential in order to maximize the energy density of the battery and to avoid lithium plating. The capacity ratio ($CR = Cap_{anode}/Cap_{cathode}$) for commercial cells ranges between 1.1 and 1.25, which means from 10% to 25% of excess of anode capacity with respect to the cathode capacity. Dubarry et al. [26] determined that in high energy (HE) cells the anode is more utilized than in high power (HP) cells. Additionally, they estimated a loading ratio of 1.1 for HE cells and 1.25 for HP cells. Accordingly, for this investigation a value of 1.1 seems to be a good approximation. Applying the mentioned loading ratio and assuming that 8–10% of the lithium in the cathode is lost to produce a stable SEI, the utilization range of the anode is between x = 0 and x = 0.8–0.82 (x in Li_xC_6).

Diverse authors [27–29] confirmed that the expansion of the graphite during the lithium intercalation does not occur linearly. Certainly, the expansion of the graphite structure is somehow related to the Li-GIC formation stages. Hahn et al. [27] measured 4% expansion of the graphite composite electrode with respect to the lithium stoichiometry. They reported a small dimension change between x = 0.2 and x = 0.6 (x in Li_xC_6) where the transformation dilute stage 1 into stage 4 takes place which is in accordance with the average variation of graphene interlayer spacing measured by Yazami et al. [29]. Due to the small variation reported for the in-plane distance (1%) [30] with the lithium intercalation, the graphite volume expansion has been assumed to vary proportionally to the graphene interlayer spacing. Additionally, the composite electrode dilatation trend has been translated into active material particle expansion assuming that 10% of the graphite [5] expansion occurs between x = 0 and x = 1. Fig. 2a) presents the expansion of the graphite with lithium intercalation (reproduced from Ref. [27]). Fig. 2b) shows the variation of the partial molar volume with the lithium intercalation. For this calculation, a maximum lithium concentration in graphite of 31.92 mol/dm^3 has been used.

A diffusion coefficient of $3.9.10^{-10}$ cm^2/s is reported in the literature for graphite at standard temperature [31]. Since the tests were performed at 35 °C, a diffusion coefficient of 6.10^{-10} cm^2/s has been used for the simulations based on the activation energy of 35 kJ/mol attributed to graphite [32].

4. Results and discussion

4.1. SEI + active material system

The results of the composed system are presented to investigate the effect of the interaction of both materials in the observed stresses.

Although the scientific community is aware of the importance of the SEI stability in the cycle life, the mechanical parameters of the SEI are almost unexplored nowadays. Very little amount of investigations have been published where they conduct experimental measurement of the mechanical properties of the SEI [16,17]. Zhang et al. [16] investigated the Young modulus of the SEI layers on MnO electrodes cycled to different voltage levels using nanoindentation technique. They reported that the Young modulus of the SEI is highly influenced by the cycled voltage level. Additionally, they detected a very large inhomogeneity in the measured values which

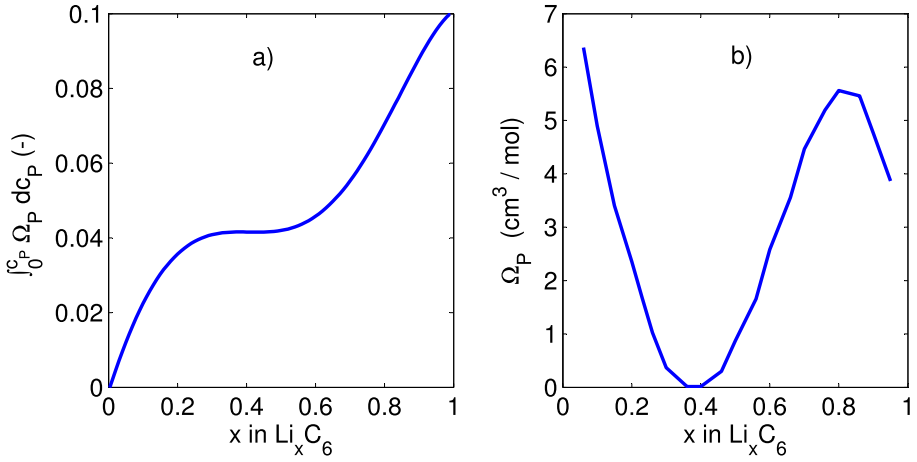

Fig. 2. a) Graphite expansion versus intercalated lithium (being c_P and Ω_P the lithium concentration in the graphite and partial molar volume respectively. P sub index refers to the active material), b) Partial molar volume versus intercalated lithium.

range from 0.01 GPa to 10 GPa.

Mechanical parameters for graphite are extensively described in the literature [5]. The simulations were carried out for an active material particle of 9 μm and a SEI layer of a 0.2 μm [15]. Since mechanical parameters of the SEI on graphite are lacking in literature, some values have to be assumed to start the sensitivity analysis. In this investigation the reported influence of voltage on the Young modulus has been neglected and a value of 0.5 GPa has been used as the SEI Young modulus, 0.2 for its Poisson's ratio and 8 MPa (which must be considerably smaller than the 30 MPa [5] of graphite) for its yield strength. In Table 2 are summarized the parameters used for the calculations. For the initial analysis in this section, a constant partial molar volume has been assumed.

For simplicity reasons, zero stress value has been assumed when the particle is in the empty state. This assumption results always in tensile stresses in the SEI layer. This would be true in the case in which the SEI layer is built at the empty state of the graphite. Despite this statement being incorrect, changing the zero stress state value in the simulations would only shift the values towards negative values. However, the results in Section 4.2 and the conclusions would remain the same because the stress amplitude would be the same (see Eq. (31)).

Fig. 3a) and b) show the comparison between the stresses calculated with the Eqs. (10) and (11) in the single active material particle and their modification due to the SEI layer interaction. Fig. 3a) corresponds to a time step in the discharge process (i.e. lithium de-intercalation from graphite) and Fig. 3b) in the charging process (i.e. lithium intercalation to graphite). The discharge and charge processes were performed at 1 C and the represented stresses correspond to a mean state of charge of 0.5 in the graphite material.

During the de-intercalation of lithium, the inner part of the particle with higher volume will exert a tensile stress on the outer part while the outer part will exert a compressive stress on the inner part of the particle (see Fig. 3a)). On the contrary, during intercalation, the inner part of the particle exerts a compressive force on the surface of the particle and the outer part a tensile stress on the core of the particle (see Fig. 3b)). The existence of the SEI layer will result in an additional compressive force in the whole particle, shifting the stress towards more negative values in both cases (intercalation and de-intercalation). However, due to the low Young modulus in the SEI layer, the stresses in the active material will be barely modified. Therefore, the modification of the stress values in the active material will strongly depend on the stiffness of the SEI layer (i.e. Young modulus). Larger Young moduli, will lead to larger compressive forces acting on the particle. Furthermore, the growth of the SEI layer would lead to material constriction in the electrode exerting an additional outer compressive force.

Fig. 3c), (de-intercalation) Fig. 3d) (intercalation) and Fig. 3e) (equilibrium state) depict the tangential and radial stresses in both: the active material and the SEI layer. The driving force for stress formation in the active material is the lithium concentration gradient; producing no stresses when the battery is at equilibrium (no concentration gradient in the active material) (see Fig. 3e)). The observed compressive stress of −0.5 MPa is the result of the interaction between the SEI and the active material. Oppositely, the stress in the SEI is not affected by the concentration gradient in the active material particle. Radial and tangential stresses in the SEI are identical in Fig. 3c), d) and e), regardless of the concentration gradient. The SEI stresses are influenced by the overall concentration inside the particle (i.e. state of charge). The large tangential stresses observed in the interface between the particle and the SEI, suggest that this location is more prone to fracture. Under the performed experimental conditions, rather mild conditions for the stresses in the active material (35 °C and 1 C), both materials are subjected to similar stresses (≈10 MPa).

The absolute stress values of both materials depend on many parameters such as the Young modulus, the diffusion coefficient, the current rate, etc…parameters that are complicate to measure making the accurate stress calculation a real challenge. It is therefore risky to affirm which material is subjected to larger stresses.

Table 2
Parameters used for the mechanical simulations.

SEI parameters				Active material parameters			
E_S (GPa)	$R_S - R_P$ (μm)	ν_S (−)	σ_{Yield} (MPa)	E_P (GPa)	R_P (μm)	ν_P (−)	Ω_P (cm^3/mol)
0.5	0.2	0.2	8	15	9	0.3	3.1

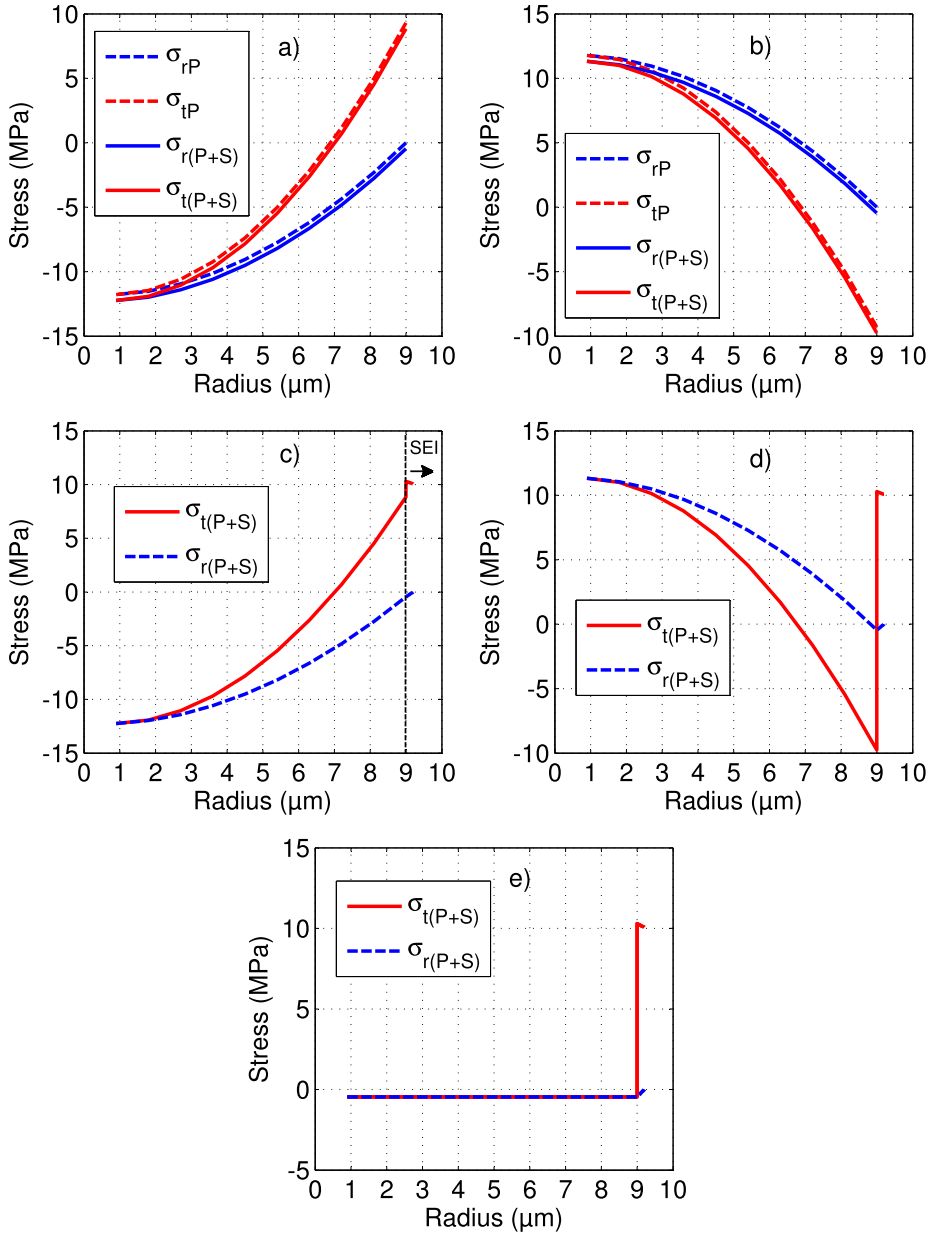

Fig. 3. Tangential (sub index *t*) and radial (sub index *r*) stresses for an average intercalated concentration of x = 0.5 (x in Li_xC_6). *P* + *S* sub index refers to the active material and SEI system, *P*, only active material. a) Stress in the active material during discharging at 1 C, b) Stress in the active material during charging at 1 C, c) Stresses in the active material and SEI during discharging at 1 C, d) Stresses in the active material and SEI during charging at 1 C, e) Stresses in the active material and SEI at equilibrium condition.

However, it seems coherent to admit, due to the porous characteristics of the SEI, that its strength is considerably smaller than the strength of the graphite active material and therefore is more likely to fracture.

The presented results show different behavior of the stress in the active material and in the SEI. The influence of the different model parameters and load conditions on the stress was quantified using a sensitivity analysis as presented by Vogler et al. [33]. In this method, each parameter has been increased by 10% from its baseline value and the change in the stress has been evaluated. The sensitivity index f_{rel} quantifies the impact of parameter *P* on the final result (maximum tangential stress in SEI $\sigma_{tS\ Max=}\ \sigma_{tS}(r = R_p)$ and tangential stress on the active material surface $\sigma_{tP\ Max\ =}\ \sigma_{tP}(r = R_p)$) and is defined as:

$$f_{rel} = \frac{\partial\sigma}{\partial P} = \frac{\frac{\sigma(P')-\sigma(P_0)}{\sigma(P_0)}}{\frac{P'-P_0}{P_0}} \tag{32}$$

In Fig. 4 the results for the sensitivity analysis are shown. The results correspond to one time step in the discharge (lithium de-intercalation from graphite) process of the full battery performed at 1 C and x = 0.5 (x in Li_xC_6).

It is worth emphasizing the large difference of the influence of the parameters on the active material particle stress and the SEI stress. While the particle size is the main contributor to the particle stress, the influence on the SEI is irrelevant. Accordingly, the C-rate and the diffusion coefficient, have a big impact on the particle stress while they play no role in the SEI stress. All these parameters influence strongly the concentration gradients inside the active

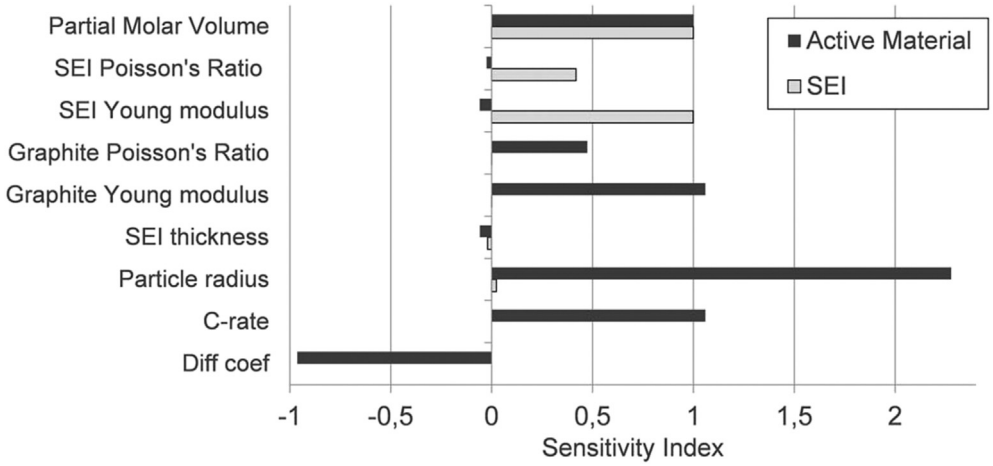

Fig. 4. Sensitivity analysis of different model parameters affecting the tangential stress in the SEI ($\sigma_{tS\ Max}$) and the tangential stress in the active material particle ($\sigma_{tP\ Max}$). The results correspond to the discharge process at 1 C and average graphite intercalated concentration of x = 0.5 (x in Li_xC_6).

material particles. This statement is valid only when performed cycles are Ah limited. Cycling limited by the voltage could lead to smaller (or larger) amount of Ah discharged or charged and thus smaller (or larger) stresses in the SEI.

As it is expected, each component (active material and SEI) is largely influenced by their mechanical parameters (Young's modulus and Poisson's ratio). However, the active material is more affected by the mechanical parameters of the SEI than the opposite. Although the higher Young modulus is detrimental for the SEI stability, the results show that it decreases the tangential stresses (i.e. leads to more compressive stresses) in the active material particle, being better for its mechanical stability. Thicker SEI results in both cases in smaller stresses, which means that the influence of the stress during cycling becomes smaller. However, in both cases the SEI thickness is not a determining factor as a small sensitivity index is observed.

The large difference in the sensitivity index of the C-rate influence on the SEI stress and the active material stress (0–1.2 respectively) could give an explanation to the spread of the data of the C-rate influence on the capacity fade reported in the literature. When it comes to the current rate influence in the aging of the Li-ion batteries, very little amount of investigations have been published in the literature. Furthermore, there is not a general agreement to describe its influence mathematically [34–36]. J. Wang et al. [36] investigated the influence of the C-rate during cycling of $LiNi_{1/3}Co_{1/3}Mn_{1/3} + LiMn_2O_4$ lithium ion batteries. On the one hand, they observed that the capacity loss increased exponentially with increasing the C-rate. On the other hand, the influence of the C-rate became smaller with increasing temperature. By this time, Purewal et al. [13] already explained this behavior based on the degradation of the SEI itself and not on the particle fracture.

It is very likely that depending on the aging conditions applied to the battery, SEI fracture or the active material fracture is the limiting factor responsible of the cell degradation. For instance, at high C-rate and low temperatures is very likely that the active material fracture contributes to the capacity loss, as high concentration gradients are expected at these conditions due to the big influence of this variables to the active material stress [14]. However, at low C-rate and medium to high temperatures, SEI fracture could be the dominant degradation mechanism.

In the following analysis, variable partial molar volume shown in Fig. 2b) has been implemented in the model. Fig. 5 shows the maximum tangential stress in the SEI layer ($\sigma_{tS\ MAX}(r = R_p)$ with the intercalation of lithium, calculated with Eq. (13)). The stress increases with the intercalated lithium in the same manner as the expansion does.

From now on, the presented analysis will always refer to the maximum tangential stress in the SEI ($\sigma_{tS}(r = R_p) = \sigma_{t\ MAX}$, calculated with Eq. (13) located in the active material SEI layer interface).

4.2. Experimental validation

As mentioned previously, the presented model has been validated with the experimental accelerated aging tests presented in Ref. [4].

Based on the reflection given in the previous sections, the predominant aging mechanism was assumed to be the loss of lithium inventory due to the break and repair effect of the SEI layer. The fracture of the SEI produced due to the active material expansion will expose the bare active material to the electrolyte leading to further reduction of the electrolyte. Due to the periodic nature of the expansion during cycling, each of the cycles will contribute to the continuous lithium consumption. Considering the aforementioned theory concerning the decrease of DIS at higher temperatures and small C-rates, particle cracking has not been taken into account in the following approach.

In Fig. 6 the experimental results of the accelerated aging tests are presented, showing the influence of DOD and SOC_{mean} on aging.

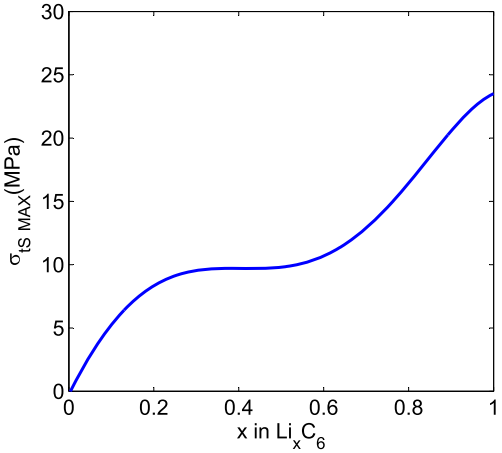

Fig. 5. Calculated maximum tangential stress in the SEI ($\sigma_{tS}(r = R_p)$ in Eq. (13)) versus intercalated lithium.

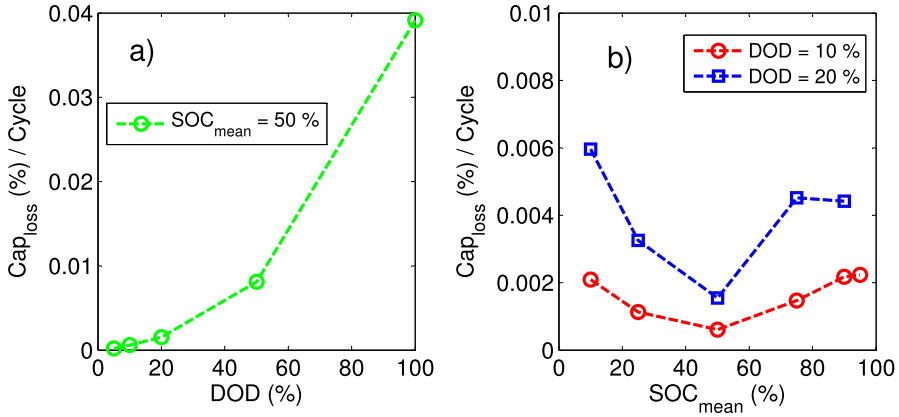

Fig. 6. Capacity loss per cycle under different cyclic conditions presented in Ref. [4]. a) Tests carried out at different DOD, 50% SOC_{mean}, at 1 C and 35 °C, b) Tests carried out at 10% and 20% DOD, different SOC_{mean} values, at 1 C and 35 °C.

For comparison with the simulations and to follow the fatigue approach presented in the Section 3.2, the capacity loss per cycle has been depicted. The total capacity loss until the end of the test has been divided by the number of cycles performed in each condition. In Fig. 6a), the influence of the DOD on the capacity loss is presented. It shows an exponential increase with the DOD that has been reported in the literature [37]. The influence of the SOC_{mean} is presented on Fig. 6b). Contrary to the calendar aging influence, which shows a bigger degradation at bigger SOC, the SOC_{mean} plays a different role during cycle aging. A parabola shaped curve behavior of capacity loss with the SOC_{mean} can be observed. A minimum of the aging is located at 50% SOC_{mean} in both cases: 20% DOD and 10% DOD. Additionally, the degradation increases symmetrically to the extreme values, with maximums at 10% SOC_{mean} and 90% SOC_{mean}.

The simulations have been carried out to reproduce the same conditions as the tests performed experimentally in order to validate the presented model. The SEI thickness increase has been neglected since the stress in the SEI shows a small dependency with its thickness. Also, the stoichiometry change in the anode during the battery aging has been neglected.

Fig. 7a) presents the tangential maximum stress value ($\sigma_{t\,Max}$) in

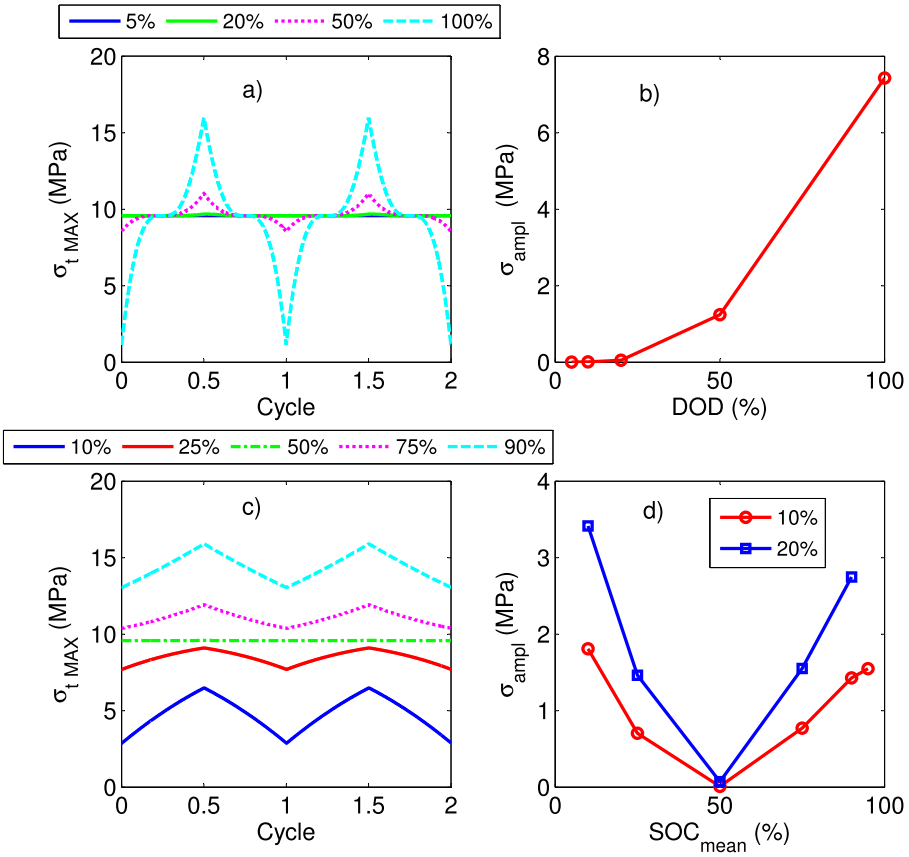

Fig. 7. a) Stress oscillations occurring during cell cycling at 50% SOC_{mean} and different DOD, at 1 C and 35 °C. The stresses correspond to the maximum tangential stress in the SEI ($\sigma_{tS\,MAX}(r = R_p)$), b) Calculated stress amplitude versus DOD, c) Stress oscillations occurring during cell cycling at 10% DOD and different SOC_{mean}, at 1 C and 35 °C, d) Stress amplitude vs. SOC_{mean} at 10% and 20% DOD.

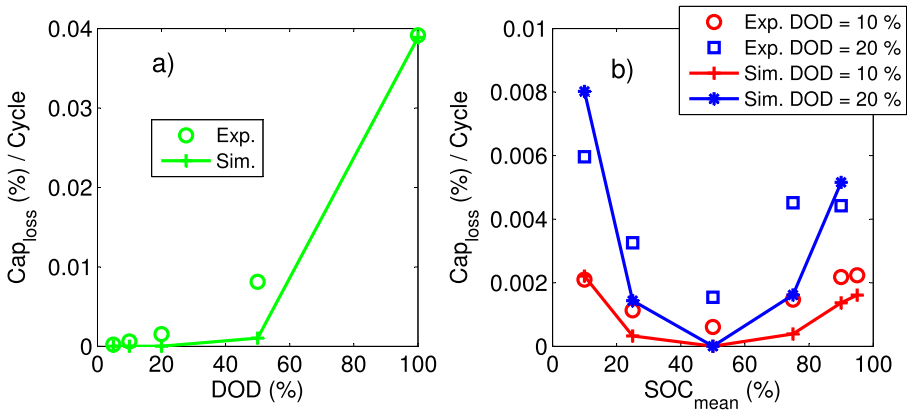

Fig. 8. Experimental capacity loss per cycle against calculated capacity loss per cycle. a) Capacity loss versus DOD for tests performed at 50% SOC_{mean} and 1 C and 35 °C, b) Capacity loss versus SOC_{mean} for 10% DOD and 20% DOD and 1 C and 35 °C.

the SEI. The simulation has been carried out maintaining 50% SOC_{mean} and varying the DOD. The trend of the stress follows a linear dependency with the expansion in the graphite. Cells cycled at DOD smaller than 20%, present very small stress oscillations due to the fact that the graphite is only cycled inside the expansion plateau (see Fig. 2a)). On the contrary, cells cycled at DOD bigger than 20%, are subjected to significantly larger stress oscillations because the graphite is cycled out from the expansion plateau. Cycles with larger DOD show a larger stress oscillation, which according to the fatigue approach presented in Section 3.2 will lead to bigger SEI damage. In Fig. 7b) are represented the stress amplitudes (defined in the Eq. (22) as half of the stress range observed in Fig. 7a)) with the variation of the DOD.

Fig. 7c) presents the stress oscillations to which the SEI is subjected to at 10% DOD and different SOC_{mean} during two cycles. The cells cycled at 10% and 90% SOC_{mean} present equivalent stress oscillations, likewise the cells cycled at 25% and 75% SOC_{mean}. However, the cell cycled at 50% SOC_{mean}, presents negligible stress amplitude. This is again the result of the behavior of the lattice parameter expansion of Fig. 2a), where the stress oscillation in the SEI is small in the expansion plateaus of the graphite.

In Fig. 7d) the stress amplitudes versus SOC_{mean} are depicted. A minimum σ_{ampl} at 50% SOC_{mean} for both cases (10% DOD and 20% DOD) will lead to less SEI damage and thus less degradation of the cell under this condition. The stress amplitudes in Fig. 7b) and d) show qualitatively good agreement with the capacity loss in the experimental data of Fig. 6.

According to the presented results, the loading ratio of the full cell plays a crucial role in the cycle aging of the battery. The presented cell with a loading ratio of 1.1 leads to a minimum stress value around 50% SOC of the battery which corresponds to 40% SOC in the graphite (see Fig. 2). Accordingly, cells manufactured with higher loading ratios the minimum cycle aging condition is expected to be shifted towards lower SOC values.

Based on the approximation presented in Section 3.2, the experimental data in Fig. 6 is fitted using the Eq. (31) and using the stress amplitudes calculated with the model (Fig. 7b) and d)). A_1 and m were treated as adjustable parameters. The fitting results for different cycling conditions are shown in Fig. 8 and the fitted parameters are summarized in Table 3.

Table 3
Fitted values for the model parameters.

A_1 (%/cycle)	m	R-square
0.04519	0.4926	0.9822

Most metals have a fatigue strength exponent close to 0.1 [38]. For instance, for steel this range can vary between 0.07 and 0.1 [39]. However, the behavior of the SEI under fatigue conditions is expected to be completely different from the usual materials reported in the literature. It has been reported that the porosity is detrimental for the strength [40,41] and fatigue life [42]. Therefore, it seems reasonable that the fatigue behavior of SEI results in much higher fatigue strength exponents, as it is in this case ($m = 0.49$). The fitting factor A_1 shows a value of 0.0452% of capacity loss per cycle. This factor does not have a crucial meaning since it is dependent on the mechanical parameters chosen for the SEI layer, such us the Young modulus, Poisson's ratio and Yield strength. The advantage of this model is that regardless the mechanical parameters of the SEI, the fitting accuracy and m factor remains constant only varying the fitting factor A_1. The good agreement between the experimental data and the model suggests that the investigation is pointing to the right direction where the mechanical degradation is the main cause for the capacity fade during cycling for the investigated cell.

5. Conclusion

A new way to explain the capacity loss during cycling has been presented in the paper. The new formalism is based on the theory of the break and repair of the SEI as the responsible effect for the cycle life degradation. Due to the volume change produced during intercalation and de-intercalation of lithium in the graphite active material, the SEI can be broken exposing bare active material to the electrolyte leading to an additional reduction of the electrolyte and thus additional SEI layer formation. In our approach, the active material degradation does not contribute significantly to the aging of the battery and consequently is not taken into account in this work.

A mechanical model of the SEI and active material composed system has been derived. The results of the model show that the DIS and SEI stress are influenced to a different extent by the material parameters of the battery as well as by the operational conditions. For example, the stress in the SEI is not influenced by the diffusion coefficient and C-rate contrary to the active material stress. Similarly, the particle size has the highest impact on the active material stress, while on the SEI stress it has a minor impact.

The mechanical model of the SEI has been implemented in a single particle lithium ion battery model. For model validation, the simulation has been compared with experimental data from accelerated aging tests with a Sanyo HE cell based on graphite/NMC technology. The model describes the DOD and SOC_{mean} influence in

the capacity fade quite well. The key parameters which characterize the influence of the DOD or SOC_{mean} on the capacity fade are the curve of the graphite expansion with the intercalated lithium and the electrode balancing. According to this investigation, the minimum degradation during cycling corresponds to the minimum stress oscillation during cycling. Hence, the minimum stress location will be affected by the balancing of the cell which determines the exact SOC at which the plateau of the graphite lattice parameter expansion is located in the full cell.

However, it has to be taken into account that under more extreme conditions such as low temperature, the active material fracture could arise as the main aging mechanism due to the dramatic decrease of the diffusion coefficient and thus an increase of the stresses.

Acknowledgment

The work has been developed in the framework of the research initiative “HGF Energie Allianz” funded by Impuls-und Vernetzungsfond der Helmholtz-Gemeinschaft e.V. Responsibility for the content of this publication lies with the authors.

References

[1] M. Kassem, J. Bernard, R. Revel, S. Pélissier, F. Duclaud, C. Delacourt, J. Power Sources 208 (2012) 296–305.
[2] J. Belt, V. Utgikar, I. Bloom, J. Power Sources 196 (2011) 10213–10221.
[3] H.J. Ploehn, P. Ramadass, R.E. White, J. Electrochem. Soc. 151 (3) (2004) A456–A462.
[4] M. Ecker, N. Nieto, S. Käbitz, J. Schmalstieg, H. Blanke, A. Warnecke, D.U. Sauer, J. Power Sources 248 (2014) 839–851.
[5] J. Christensen, J. Newman, J. Solid State Electrochem. 10 (2006) 293–319.
[6] J. Christensen, J. Newman, J. Electrochem. Soc. 153 (6) (2006) A1019–A1030.
[7] J. Christensen, J. Electrochem. Soc. 157 (3) (2010) A366–A380.
[8] S. Renganathan, G. Sikha, S. Santhanagopalan, R.E. White, J. Electrochem. Soc. 157 (2) (2010) A155–A163.
[9] X. Zhang, W. Shyy, A.M. Sastry, J. Electrochem. Soc. 154 (10) (2007) A910–A916.
[10] J. Park, W. Lu, A.M. Sastry, J. Electrochem. Soc. 158 (2) (2011) A201–A206.
[11] Y. Qi, H. Guo, L.G. Hector Jr., A. Timmons, J. Electrochem. Soc. 157 (5) (2010) A558–A566.
[12] R. Deshpande, M. Verbrugge, Y.-T. Cheng, J. Wang, P. Liu, J. Electrochem. Soc. 159 (10) (2012) A1730–A1738.
[13] J. Purewal, J. Wang, J. Graetz, S. Soukiazian, H. Tataria, M.W. Verbrugge, J. Power Sources 272 (2014) 1154–1161.
[14] K. Takahashi, V. Srinivasan, J. Electrochem. Soc. 162 (4) (2015) A635–A645.
[15] P. Verma, P. Maire, P. Novák, Electrochim. Acta 55 (2010) 6332–6341.
[16] J. Zhang, R. Wang, X. Yang, W. Lu, X. Wu, X. Wang, H. Li, L. Chen, Nano Lett. 12 (2012) 2153–2157.
[17] H. Shin, J. Park, S. Han, A.M. Sastry, W. Lu, J. Power Sources 277 (2015) 169–179.
[18] M. Winter, J.O. Besenhard, M.E. Spahr, P. Novák, Adv. Mater. 10 (1998) 10.
[19] F. Hao, D. Fang, J. Electrochem. Soc. 160 (4) (2013) A595–A600.
[20] Y-T. Cheng, M.W. Verbrugge, J. Appl. Phys. 104 (2008) 083521.
[21] O.H. Basquin, ASTM 10 (1910) 625–630.
[22] M.A. Miner, J. Appl. Mech. 67 (1945) A159–A164.
[23] J. Schmalstieg, S. Käbitz, M. Ecker, D.U. Sauer, J. Power Sources 257 (2014) 325–334.
[24] S. Santhanagopalan, Q. Guo, P. Ramadass, R.E. White, J. Power Sources 156 (2006) 620–628.
[25] M. Guo, G. Sikha, R.E. White, J. Electrochem. Soc. 158 (2) (2011) A122–A132.
[26] M. Dubarry, C. Truchot, B.Y. Liaw, J. Power Sources 258 (2014) 408–419.
[27] M. Hahn, H. Buqa, P.W. Ruch, D. Goers, M.E. Spahr, J. Ufheil, P. Novák, R. Kötz, Electrochem. Solid State Lett. 11 (9) (2008) A151–A154.
[28] V.A. Sethuraman, N. Van Winkle, D.P. Abraham, A.F. Bower, P.R. Guduru, J. Power Sources 206 (2012) 334–342.
[29] R. Yazami, Y. Reyner, J. Power Sources 153 (2006) 312–318.
[30] D. Billaud, F.X. Henry, M. Lelaurain, P. Willmann, J. Phys. Chem. Solids 57 (1996) 775–781.
[31] L.H. Saw, Y. Ye, A.A.O. Tay, Energy Convers. Manag. 75 (2013) 162–174.
[32] T.L. Kulova, A.M. Skundin, E.A. Nizhnikovskii, A.V. Fesenko, Russ. J. Electrochem. 42 (3) (2006) 259–262.
[33] M. Vogler, A. Bieberle-Hütter, L. Gauckler, J. Warnatz, W.G. Bessler, J. Electrochem Soc. 156 (5) (2009) B663–B672.
[34] K. Takei, K. Kumai, Y. Kobayashi, H. Miyashiro, N. Terada, T. Iwahori, T. Tanaka, J. Power Sources 97–98 (2001) 697–701.
[35] J. Wang, P. Liu, J. Hichs-Garner, E. Sherman, S. Soukiazian, M. Verbrugge, H. Tataria, J. Musser, P. Finamore, J. Power Sources 196 (2011) 3942–3948.
[36] J. Wang, J. Purewal, P. Liu, J. Hicks-Garner, S. Soukazian, E. Sherman, A. Sorenson, L. Vu, H. Tataria, M.W. Verbrugge, J. Power Sources 269 (2014) 937–948.
[37] S.B. Peterson, J. Apt, J.F. Whitacre, J. Power Sources 195 (2010) 2385–2392.
[38] N.A. Fleck, K.J. Kang, M.F. Ashby, Acta Metall. Mater 42 (2) (1994) 365–382.
[39] B. Boardman, ASM Handbook, vol. 1, 1990, pp. 673–688.
[40] H. Zheng, L. Tan, G. Liu, X. Song, V.S. Battaglia, J. Power Sources 208 (2012) 52–57.
[41] H. Zheng, L. Zhang, G. Song, X. Song, V.S. Battaglia, J. Power Sources 217 (2012) 530–537.
[42] Y. Yan, G.L. Nash, P. Nash, Int. J. Fatigue 55 (2013) 81–91.